Highly birefringent phase-shifted fiber Bragg gratings inscribed with femtosecond laser

Jun He,[1] Yiping Wang,[1,*] Changrui Liao,[1] Qiaoni Wang,[2] Kaiming Yang,[1] Bing Sun,[1] Guolu Yin,[1] Shen Liu,[1] Jiangtao Zhou,[1] and Jing Zhao[1]

[1]*Key Laboratory of Optoelectronic Devices and Systems of Ministry of Education and Guangdong Province, College of Optoelectronic Engineering, Shenzhen University, Shenzhen 518060, China*

[2]*Key Laboratory on Precision Opto-Mechatronics Technology of the Ministry of Education, Beihang University, Beijing 100191, China*

**Corresponding author: ypwang@szu.edu.cn*

Received February 4, 2015; revised March 25, 2015; accepted April 1, 2015; posted April 2, 2015 (Doc. ID 233813); published April 24, 2015

We demonstrate a highly birefringent phase-shifted fiber Bragg grating (PS-FBG) inscribed in H_2-free fiber with a near-infrared femtosecond Gaussian laser beam and uniform phase mask. The PS-FBG was fabricated from an ordinary fiber Bragg grating (FBG) in a case in which overexposure was applied. The spectral evolution from FBG to FS-FBG was observed experimentally with a decrease in transmission loss at dip wavelength, blueshift of the dip wavelength, decrease in the cladding mode loss, and an increase in the insertion loss. A high birefringence was demonstrated experimentally with the existence of PS-FBG only in TM polarization. The formation of the PS-FBG may be due to a negative index change induced by the higher intensity in the center of the Gaussian laser beam.

OCIS codes: (060.3735) Fiber Bragg gratings; (320.7110) Ultrafast nonlinear optics; (350.3390) Laser materials processing.

http://dx.doi.org/10.1364/OL.40.002008

Phase-shifted fiber Bragg gratings (PS-FBGs) have a wide range of applications in the areas of fiber lasers, optical networks, microwave photonics, and fiber-optic sensors. They can be used as the cavities of distributed feedback (DFB) fiber lasers [1,2], high-fineness tunable optical filters [3,4], high-resolution strain sensors, and refractive index sensors [5]. Numerous techniques have been developed for PS-FBG fabrication, such as the moving fiber-scanning beam method [2], shielded phase mask method [4], creation of internal microstructures [5], point-by-point inscription [6], and post-processing by applying localized exposure to UV or CO_2 lasers [7,8]. However, these methods are complex, expensive, and always need additional apparatus.

In the past decade, femtosecond lasers have been explored for fiber Bragg grating (FBG) inscription in various fibers [9–18]. Nonlinear index change induced by near-infrared (NIR) femtosecond laser was observed both in type I and type II gratings [11–14]. A five-photon absorption process, together with an index change threshold and index saturation level, was reported in the formation of type I gratings [11]. A positive index change and low birefringence were induced in type I gratings by low-intensity laser pulses, whereas a negative index change and high birefringence were induced in type II gratings by high-intensity pulses [15–17]. Moreover, a high birefringence of 8×10^{-4} was achieved by post-exposing the FBG cladding [17]. The laser-induced nonlinear index change, which was positive at a lower intensity and negative at a higher intensity, may provide a novel method to fabricate PS-FBGs with a femtosecond Gaussian laser beam and uniform phase mask.

In this Letter, we demonstrate a highly birefringent PS-FBG inscribed in H_2-free fiber with a NIR femtosecond Gaussian laser beam and uniform phase mask. The PS-FBG was fabricated from an ordinary FBG in a case in which overexposure was applied. The spectral evolution from FBG to FS-FBG was observed experimentally with a decrease in the transmission loss at dip wavelength, blueshift of the dip wavelength, decrease in the cladding mode (CM) loss, and an increase in the insertion loss. A high birefringence was demonstrated with the existence of PS-FBG only in TM polarization. The formation of PS-FBG may result from a negative index change induced by the higher intensity in the center of the Gaussian laser beam.

The experimental setup used for fabricating FBGs and PS-FBGs is similar to that presented in a previous work [16]. Femtosecond laser pulses with a wavelength of 800 nm, pulse width of 100 fs, repetition rate of 1 kHz, and pulse energy of 4 mJ were generated by a Ti:sapphire regenerative amplifier system (Spectra-Physics, Solstice). The laser was linearly polarized with a $1/e^2$ Gaussian diameter of 6.2 mm. The pulse energy was attenuated by rotating a half-wave plate followed by a Glan polarizer. The laser beam was focused onto the fiber core using a cylindrical lens with a focal length of 50.2 mm through a uniform phase mask (Ibsen Photonics), which had a period of 1070 nm, 0th order diffraction of below 4%, and an optimization for 800 nm TE illumination. Standard Corning SMF-28 fiber with coating removed was fixed behind the phase mask at a distance of 300 μm. Using Gaussian beam optics, the focal width and Rayleigh length of the laser beam were calculated to be 8.25 and 66.78 μm, respectively. Transmission and reflection spectra were measured online using a broadband light source together with an optical spectrum analyzer (Yokagawa AQ6370C).

At first, an ordinary FBG with a transmission loss of –21.35 dB was inscribed in H_2-free fiber with a pulse energy of 220 μJ (i.e., laser peak intensity of 8.2×10^{12} W/cm^2) and exposure time of 60 s. The original FBG was further exposed to a femtosecond laser with the same pulse energy for another 180 s. In this period,

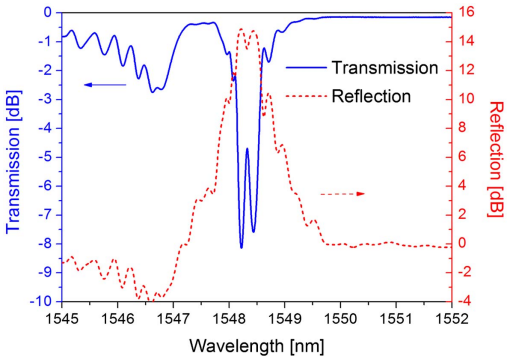

Fig. 1. Transmission and reflection spectra of PS-FBG fabricated from an ordinary FBG in case in which overexposure to NIR femtosecond laser was applied (H_2-free Corning SMF-28 fiber; pulse energy, 220 μJ; exposure time, 240 s).

the FBG degenerated with the emergence of a phase-shifted peak. A PS-FBG was finally obtained after a total exposure time of 240 s. As shown in Fig. 1, a phase-shifted peak at the wavelength of 1548.33 nm can be seen within the stop-band of the FBG transmission spectrum, and a phase-shifted dip can be observed in the reflection spectrum. It should be noted that 0 dB in the reflection spectrum is the Fresnel reflection of fiber end of about 4%. Moreover, the out-of-band insertion loss of the PS-FBG is 0.25 dB at the wavelength of 1550.00 nm.

The growth of the PS-FBG was monitored by recording the transmission spectra at an interval of 30 s. It can be seen from Fig. 2 that the process of PS-FBG fabrication

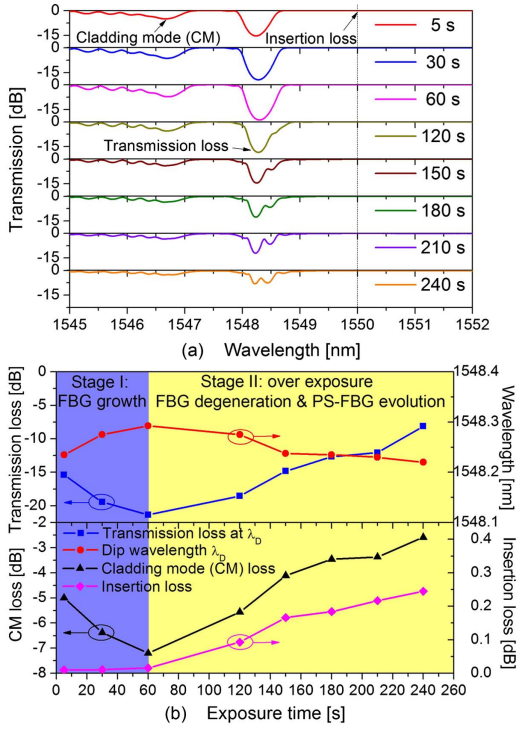

Fig. 2. (a) Evolution of transmission spectrum from original FBG to PS-FBG in case in which overexposure to femtosecond laser was applied. (b) Transmission loss and dip wavelength λ_D of the FBG (upper panel), and cladding mode (CM) and insertion loss at 1550.00 nm (lower panel) as a function of exposure time.

can be divided into two stages: normal FBG growth at stage I (0–60 s) and abnormal overexposure at stage II (60–240 s). At stage I, the transmission loss at dip wavelength λ_D and the CM loss increase with a redshift of the dip wavelength. The out-of-band insertion loss at 1550.00 nm grows slowly and is very small (<0.05 dB) at this stage. At stage II, the FBG degenerates gradually with the emergence and evolution of the PS-FBG. The transmission and CM loss decrease with a blueshift of the dip wavelength and phase-shifted peak. The out-of-band insertion loss at stage II grows faster and becomes much larger (up to 0.25 dB) than that at stage I.

Further experiments were carried out to evaluate the repeatability of PS-FBG fabrication and the influence of laser intensities and hydrogen loading. Four PS-FBGs (FBGs 2–5) were successfully inscribed in H_2-free fiber with the same pulse energy of 220 μJ. Another PS-FBG (FBG 1) was fabricated with a slightly higher pulse energy of 240 μJ. Degenerations of FBGs 1–5 can be seen in Fig. 3 in cases of overexposure. Moreover, different degeneration rates and transmission losses are observed in the evolutions of FBGs 2–5, which were inscribed with the same pulse energy. The differences in degeneration may result from the threshold effect of laser-induced negative index change, which can easily be affected by fiber uniformity, focusing accuracy, and laser power fluctuations.

FBGs 6–7 and FBG 8 were inscribed in H_2-free fiber with lower pulse energies of 180 and 140 μJ, respectively. As shown in Fig. 3, FBGs 6–8 grow much slower than FBGs 1–5, and no degeneration occurs in cases of overexposure. The lower-energy laser pulses were insufficient to induce negative index changes, and hence PS-FBGs could not be fabricated from FBGs 6–8.

Moreover, PS-FBGs also could not be fabricated from FBGs 9–10, which were inscribed in H_2-loaded fiber (H_2-loading at 100 bar, 80°C, for 7 days) with pulse energies of 220 and 140 μJ, respectively. Both FBGs 9 and 10 grew very fast at the beginning and saturated at a transmission loss of around −47.50 dB without any degeneration in cases of overexposure. The difference in the evolutions of FBG 9 (H_2-loaded) and FBGs 2–5 (H_2-free), which

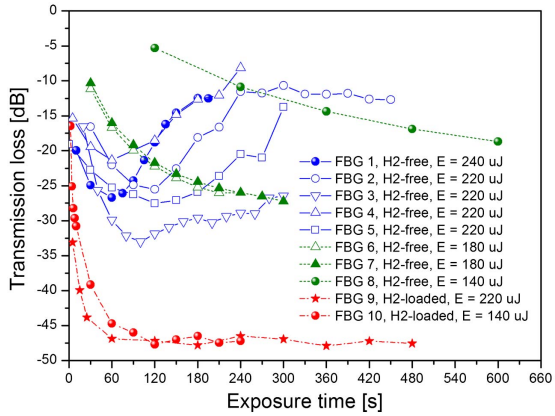

Fig. 3. Evolution of the transmission loss at dip wavelength as a function of exposure time for the FBGs inscribed in H_2-free and H_2-loaded fibers with different laser pulse energies. Degeneration only occurred in H_2-free fibers with higher pulse energies.

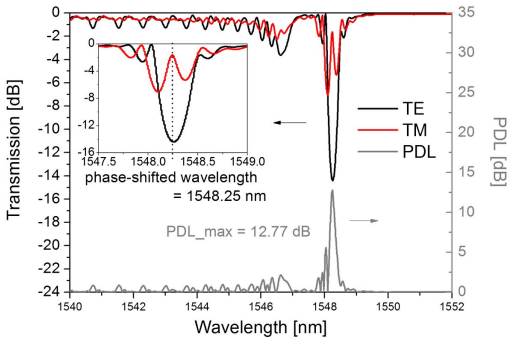

Fig. 4. Transmission spectra of two orthogonal linear polarization modes (TE and TM), and PDL spectrum of the PS-FBG.

were inscribed with the same pulse energy, may be due to the different mechanisms of grating formation in H_2-loaded and H_2-free fibers. The index change profile in H_2-free fiber is more sensitive to laser intensity than that in H_2-loaded fiber [13]. The different types, quantities, and distributions of laser-induced defects will introduce different stress distributions across the fiber cores of H_2-loaded and H_2-free fibers, and thus induce different index changes due to the photoelastic effect [18–20]. As a result, PS-FBGs can only be fabricated in H_2-free fiber with higher pulse energies.

The transmission spectra of two orthogonal linear polarization modes (TE and TM) and the polarization-dependent loss (PDL) of the PS-FBG were measured by an optical component analyzer, which was composed of a tunable laser source (Agilent, 81940A), polarization synthesizer (Agilent, N7786B), and an optical power meter (Agilent, N7744A). As shown in Fig. 4, the PS-FBG only exists in TM polarization, whereas a normal FBG spectrum is shown in TE polarization. Moreover, the maximum PDL was measured to be 12.77 dB at the central wavelength of 1548.25 nm.

The birefringence and polarization dependence of the PS-FBG were further investigated as shown in Fig. 5(a). The tunable laser generated a single-polarized laser with a wavelength of 1548.25 nm and power of 6.92 dBm. The polarization synthesizer generated and stabilized a pair of orthogonal linear polarization states P1 and P2 separately. The normalized Stokes vectors of P1 and P2 are [1.000, 0.005, −1.001, 0.006] and [1000, 0.004, 1.004, 0.005], respectively, as demonstrated on the Poincaré sphere in Fig. 5(b). The end face of the PS-FBG was cleaved and then fixed under an optical microscope (Leica, DM 2500M). The near mode field profiles of P1 and P2 after transmission in the PS-FBG were measured by an infrared camera (Electro Physics, 7290A). As shown in Fig. 5(c), a high-intensity LP01 mode profile is observed for polarization P1 at the wavelength within the FBG stop-band, whereas almost no light can be detected for polarization P2. As a result, the PS-FBG is highly birefringent at the central wavelength.

The spectral evolution of TE and TM polarizations was investigated during PS-FBG fabrication. A PS-FBG was fabricated in H_2-free fiber with pulse energy of 220 μJ and exposure time of 210 s. The transmission spectra of TE and TM polarizations were measured online by the optical component analyzer. As shown in Fig. 6(a), the degeneration of FBG and the spectral evolution from FBG to PS-FBG mainly occur in TM polarization. The original FBG, which was inscribed with an exposure time of 30 s, has a slightly larger transmission loss at a slightly shorter dip wavelength in TM polarization. Therefore, a larger index modulation depth and smaller average index change (i.e., a sharper index profile) are expected in TM polarization than in TE polarization of the original FBG. In cases of overexposure, a phase-shifted peak emerges within the FBG stop-band from the longer wavelength side. The transmission loss in TM polarization decreases from −26.90 to −11.31 dB with a blueshift of the dip wavelength of about 0.11 nm, whereas the decrease of transmission loss is much smaller in TE polarization (i.e., from −26.96 to −22.69 dB). Moreover, the maximum PDL of the PS-FBG is 20.02 dB during fabrication.

The transition from the original FBG to the highly birefringent PS-FBG may result from the nonlinear index change and high birefringence induced by the femtosecond laser. In previous works [15,21], negative index change and high birefringence were demonstrated both

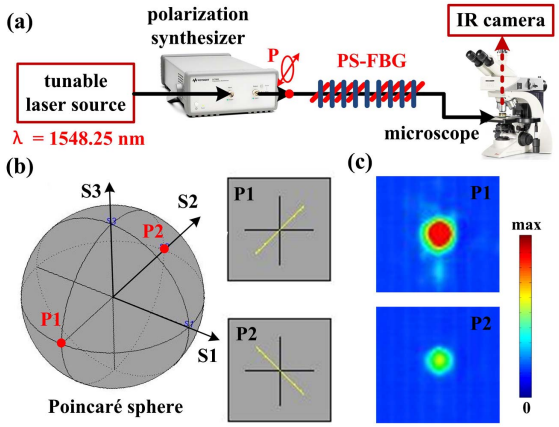

Fig. 5. Measurement of near mode field profiles of two orthogonal linear polarization states (P1 and P2) after transmission in the PS-FBG. (a) Experimental setup. (b) Generation of P1 and P2 shown on the Poincaré sphere. (c) Measured near mode field profiles of P1 and P2.

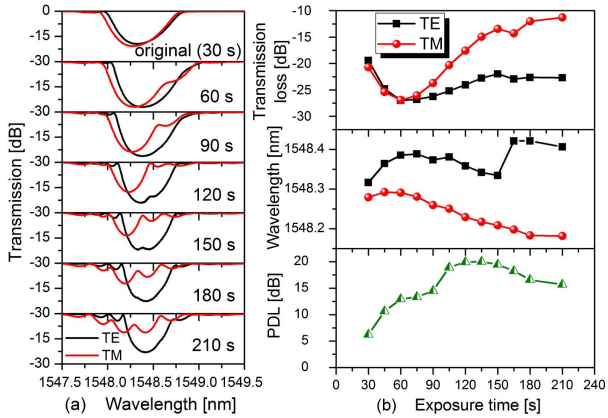

Fig. 6. (a) Transmission spectrum evolutions of two orthogonal polarization modes (TE and TM) during PS-FBG fabrication. (b) Transmission losses and dip wavelengths of the TE/TM transmission spectra and PDL of the PS-FBG as a function of exposure time.

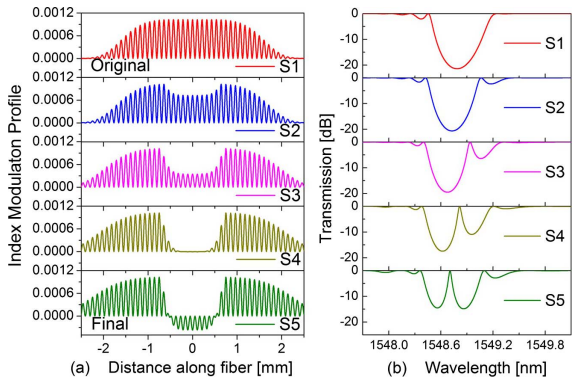

Fig. 7. (a) Index profile models of the PS-FBG at different fabrication stages from S1 to S5 (S1, the original FBG; S5, the final PS-FBG; the grating pitches are exaggerated 200 times for clarity). (b) Corresponding transmission spectra calculated by use of coupled-mode theory and transfer matrix method.

in type II gratings and silica glass written by high-intensity NIR femtosecond laser pulses. The laser-induced asymmetric stress across the fiber core will decrease the refractive index and increase the birefringence due to the photoelastic effect [19,20]. As a result, the much higher intensity in the center of Gaussian beam may introduce a negative index change in the middle of a FBG (i.e., "erased" by overexposure), forming a Fabry–Perot structure or a PS-FBG. Moreover, the negative index change only exists in the polarization parallel to the laser incident direction.

It can be seen from Figs. 2 and 6 that the evolution of PS-FBG is accompanied by a decrease in the transmission loss at dip wavelength, blueshift of the dip wavelength, decrease in the CM loss, and an increase in the insertion loss. The decrease in the CM loss excludes the possibility of FBG inscription in the fiber cladding or cladding/core interface [17,22]. The decrease in transmission loss, blueshift of the dip wavelength, and increase in insertion loss all indicate that a negative index change does exist within the PS-FBG.

According to the analysis, a qualitative simulation was carried out with the index profiles of PS-FBG at different fabrication stages modeled in Fig. 7(a). The corresponding transmission spectra were calculated by use of coupled-mode theory and transfer matrix method [23]. It can be observed from Figs. 2(a), 6(a), and 7(b) that the measured spectral evolution of the PS-FBG agrees well with the simulated result. It should be noted that the real index profiles of the PS-FBGs in the experiments should be far more complicated than in the models.

In summary, a highly birefringent PS-FBG was fabricated from an overexposed FBG inscribed in H_2-free fiber with a NIR femtosecond laser and uniform phase mask. The spectral evolution from FBG to FS-FBG was observed with a decrease in the transmission loss at dip wavelength, blueshift of the dip wavelength, decrease in the cladding mode (CM) loss, and an increase in the insertion loss. A high birefringence with the existence of PS-FBG only in TM polarization was experimentally demonstrated. Simulations showed that the PS-FBG may be due to a negative index change induced by the higher intensity in the center of the Gaussian laser beam. Such a PS-FBG could be used to develop a promising tunable optical filter or a single-polarized DFB fiber laser.

This work was supported by the National Natural Science Foundation of China (grant nos. 61425007, 11174064, 61377090, and 61308027), the Natural Science Foundation of Guangdong (2014A030308007 and 2014A030312008), the Science & Technology Innovation Commission of Shenzhen/Nanshan (grant nos. KQCX20120815161444632, JCYJ20130329140017262, ZDSYS20140430164957664, and KC2014ZDZJ0008A), and the Pearl River Scholar Fellowships.

References

1. M. N. Zervas, R. Wilmshurst, and L. M. B. Walker, Opt. Lett. **38**, 1533 (2013).
2. H. F. Qi, Z. Q. Song, S. J. Li, J. Guo, C. Wang, and G. D. Peng, Opt. Express **21**, 11309 (2013).
3. B. Lin, M. Jiang, S. C. Tjin, and P. Shum, IEEE Photon. Technol. Lett. **23**, 1292 (2011).
4. S. Rota-Rodrigo, L. Rodriguez-Cobo, M. A. Quintela, J. M. Lopez-Higuera, and M. Lopez-Amo, IEEE J. Sel. Top. Quantum. Electron. **20**, 161 (2014).
5. C. R. Liao, L. Xu, C. Wang, D. N. Wang, Y. P. Wang, Q. Wang, K. M. Yang, Z. Y. Li, X. Y. Zhong, J. T. Zhou, and Y. J. Liu, Opt. Lett. **38**, 4473 (2013).
6. J. Burgmeier, C. Waltermann, G. Flachenecker, and W. Schade, Opt. Lett. **39**, 540 (2014).
7. J. Canning and M. G. Sceats, Electron. Lett. **30**, 1344 (1994).
8. L. Xia, P. Shum, and C. Lu, Opt. Express **13**, 5878 (2005).
9. S. J. Mihailov, D. Grobnic, C. W. Smelser, P. Lu, R. B. Walker, and H. M. Ding, Opt. Mater. Express **1**, 754 (2011).
10. Y. P. Wang, H. Bartelt, M. Becker, S. Brueckner, J. Bergmann, J. Kobelke, and M. Rothhardt, Appl. Opt. **48**, 1963 (2009).
11. C. W. Smelser, S. J. Mihailov, and D. Grobnic, Opt. Express **13**, 5377 (2005).
12. C. W. Smelser, S. J. Mihailov, and D. Grobnic, J. Opt. Soc. Am. B **23**, 2011 (2006).
13. C. W. Smelser, S. J. Mihailov, and D. Grobnic, Opt. Lett. **32**, 1453 (2007).
14. C. W. Smelser, S. J. Mihailov, and D. Grobnic, J. Opt. Soc. Am. B **25**, 877 (2008).
15. P. Lu, D. Grobnic, and S. J. Mihailov, J. Lightwave Technol. **25**, 779 (2007).
16. C. R. Liao, Y. H. Li, D. N. Wang, T. Sun, and K. T. V. Grattan, IEEE Sens. J. **10**, 1675 (2010).
17. D. Grobnic, S. J. Mihailov, and C. W. Smelser, J. Lightwave Technol. **25**, 1996 (2007).
18. N. Troy, C. W. Smelser, and D. M. Krol, Opt. Mater. Express **2**, 1663 (2012).
19. F. Durr, H. G. Limberger, R. P. Salathe, F. Hindle, M. Douay, E. Fertein, and C. Przygodzki, Appl. Phys. Lett. **84**, 4983 (2004).
20. H. G. Limberger, P. Y. Fonjallaz, R. P. Salathe, and F. Cochet, Appl. Phys. Lett. **68**, 3069 (1996).
21. E. Bricchi, B. G. Klappauf, and P. G. Kazansky, Opt. Lett. **29**, 119 (2004).
22. Q. Z. Rong, X. G. Qiao, T. Guo, W. J. Bao, D. Su, and H. Z. Yang, Opt. Lett. **39**, 6616 (2014).
23. T. Erdogan, J. Lightwave Technol. **15**, 1277 (1997).